Supporting Material

Mathematical Modeling and Validation of Glucose Compensation of the Neurospora Circadian Clock

Andrey A. Dovzhenok,[1] Mokryun Baek,[2] Sookkyung Lim,[1] and Christian I. Hong[2]*

[1]Department of Mathematical Sciences, University of Cincinnati, Cincinnati, Ohio;
and [2]Department of Molecular and Cellular Physiology, University of Cincinnati College of Medicine, Cincinnati, Ohio

*Correspondence: christian.hong@uc.edu

Table of contents

1. SUPPORTING TEXT

Text S1. Selection of Hill coefficients and other model assumptions

It is known that stronger nonlinearity favors oscillations with a larger oscillatory domain (see, for example, (1)). Our simulations revealed that the increasing Hill coefficient of WC-1 activating *frq* produces larger period variations with the change in the *wc-1* transcription (k_7) or the WC-1 translation (k_8) rate constants (Fig. S1, *A* and *B*). Higher cooperativity of WC-1 activation of *frq* transcription leads to stronger nonlinearity in the model that produces sharper and larger increases of FRQ_n levels (Fig. S1, *C* and *D*). This is a critical observation for understanding how increased cooperativity of WC-1 activation of *frq* transcription influences the period in the model since FRQ_n plays a major role in changing the period (see Fig. S10 and Text S2 for more details) that was observed in overexpression and glucose experiments (2, 3). Higher reaction order (r = 2) of FRQ_c positive feedback on WC-1 translation is likely as FRQ is known to form homodimers (4). This high cooperativity also increased the period change in the model, although this increase was moderate compared to the increase due to higher cooperativity of WC-1 activating *frq* transcription. Ultimately, we explored different reaction orders for the Hill type functions discussed above with the combination used in this study (see model equations) eventually producing the best fit to the existing experimental data with the lowest possible cooperativity.

In this study, a relatively high reaction order (n = 6) of WC-1 activation of *frq* transcription is essential to simulate the existing experimental data on period variation. This high reaction order may be necessary to compensate for the insufficient nonlinearity in the simplified model we considered in this paper. In particular, our model does not include various reported post-translational modifications and interactions of the core clock components. For example, it is still unclear what role the experimentally observed progressive phosphorylation of FRQ (5) or the coiled-coil domain-mediated FRQ-FRQ interaction (4) play in the Neurospora circadian clock. Furthermore, the peak of FRQ was estimated to lag behind the peak of *frq* mRNA by about 4-6 hours (5) which suggests a delay in FRQ translation. If incorporated in the model, these regulatory interactions may increase overall nonlinearity and allow lower reaction order/Hill coefficient of WC-1 activation of *frq* transcription. However, they would also make equations

considerably more complex and therefore we do not include these post-translational modifications in the current simplified Neurospora circadian clock model.

Likewise, experimental observations suggest some post-translational modifications/interactions during WC-1 binding at the *frq* promoter. For example, the time between the peaks of WC-1 and FRQ was estimated from experimental data to be around 12 h (6). As we mentioned earlier, the peak of *frq* mRNA was reported to precede the peak of FRQ protein by about 4-6 hours (5) which means that the peak of *frq* mRNA happens about 6-8 hours after the peak of WC-1. Hence, there is either a delayed binding of WC-1 at the *frq* promoter or the transcription of *frq* does not start immediately after binding of WC-1 at the aforementioned promoter. In any case, the exact origin of observed delay remains unknown.

One notable property of the model is that one-parameter period diagrams for expression and translation rate constants of either *frq* or *csp-1* have identical shapes (although the parameter range of the two diagrams may be different). This property also holds for expression and translation rate constants k_7/k_8 of *wc-1* when the rate of change of cytosolic WC-1 ($d[\text{WC-1}_c]/dt$) is linearly dependent on the concentration of *wc-1* mRNA (see model equations in (7)). In contrast, when WC-1_c synthesis shows saturation kinetics in *wc-1* mRNA (as we model it in the current study) the period with the increase in parameter k_7 levels off at around 20 h and the period diagram is significantly different from the diagram in parameter k_8 (compare Fig. 4 *A* and Fig. S10 *A*). Our modeling results, experimental data on *wc-1* overexpression (2) and the fact that only decrease of the period was observed with the increase in glucose concentration in *csp-1*^{ko} strain (3) may indicate the existence of a *wc-1* mRNA saturation mechanism for WC-1 translation in Neurospora clock. Moreover, this modeling result also suggests that the increased abundance of WC-1 protein observed experimentally in *csp-1*^{ko} strains (3) is mainly due to the increased *wc-1* gene expression and not the increased translation rate.

Text S2. Regulation of clock period

A periodic solution in the *wc-1* transcription rate constant k_7 in the simulated *csp-1*^{ko} strain appears from the Hopf bifurcation (Fig. 4, *B* and *C*). However, the oscillatory range is unbounded from above due to saturation of WC-1 accumulation w.r.t. *wc-1* mRNA that we include in our model (see model equations). In contrast to the diagram in the rate constant k_7, the oscillatory region in the rate constant k_8 is bounded by the two Hopf bifurcations (Fig. S10, *B*

and *C*). Clock period in a close vicinity of the Hopf bifurcations follows the change in the amplitudes of FRQ_n or WC-1_n (Fig. S10). The same relationship between period and amplitude is observed in the model during initial period increase in the *wc-1* overexpression experiment in the *wc-1*^{ko} strain (Fig. 3 *C*) and during period decrease observed in the *csp-1* overexpression simulations (Figs. 3 *D* and S5 *A*). The characteristic feature of all these oscillatory regimes is low abundance of FRQ_n (Figs. 4B, S3 *B*, S5 *B* and S10 *B*) that is not sufficient to fully inactivate WC-1_n. This leads to low amplitude of WC-1_n oscillations (Figs. 4 *C*, S5 *C* and S10 *C*). In contrast, period changes away from the Hopf bifurcation points are almost inversely related to changes in the amplitude of FRQ_n (Fig. S10, *A* and *B*), although this correlation is not perfect as other variables also influence the period in the model. In contrast to FRQ_n, WC-1_n amplitude does not have an apparent relationship with the period away from the two Hopf bifurcations (Figs. 4 *C* and S10 *C*). Therefore, the vertical dashed lines in Fig. S10 that mark the peaks in the period curves may be considered the boundaries between the FRQ_n-regulated regime away from the Hopf bifurcations and low-amplitude regime in the vicinity of the Hopf bifurcations.

To explain the mechanism of how FRQ_n regulates the period in the model we turn to oscillatory profiles of WC-1_n and FRQ_n. When the rate of WC-1 translation (k_8) is relatively low it takes more time to accumulate WC-1 in the nucleus to start *frq* transcription and the period is long (Fig. S11 *A*). Increase in the WC-1 translation rate leads to faster accumulation of WC-1 in the nucleus and higher amplitude of WC-1_n oscillations (Fig. S11). High amplitude of WC-1_n oscillations triggers a sharp increase in *frq* mRNA abundance due to cooperativity of WC-1_n activation of *frq* transcription. This, in turn, results in rapid growth of the amplitude of FRQ_n oscillations and the accelerated clearance of WC-1 from the nucleus via complex formation with FRQ (Fig. S11 *B*). Faster WC-1 accumulation in the nucleus together with faster WC-1 clearance from the nucleus contribute to a dramatic decrease in the period when the parameter k_8 is moderately increased in the model (Fig. S11 *B*). Further increase in the rate of WC-1 translation results in an even higher WC-1_n amplitude (Figs. S10 *C* and S11 *C*). Since the model assumes degradation of WC-1_n (WCC) as a complex with FRQ_n (see model equations), the increasing WC-1_n abundance eventually starts to erode FRQ_n levels (Fig. S11, *C* and *D*). High abundance of WC-1_n and low abundance of FRQ_n lead to slower inactivation and removal of WC-1 from the nucleus (Fig. S11 *C*) and, ultimately, a longer period (Fig. S10 *A*).

Similar FRQ_n-regulated period change behavior is observed in the simulated WT strain after reinstatement of the negative feedback via *csp-1* in the model (Fig. S12). This result is expected because in both cases the increase in k_7 leads to higher abundance of WC-1 (Figs. 4 *C* and S12 *E*) which is the rate-limiting factor of the WCC and expression level of the WCC was found experimentally to determine the period of the circadian clock (2). In the *csp-1*^{ko} there is no inhibition of *wc-1* expression by CSP-1 and we simulate higher glucose levels by increasing parameter k_7 observing a decreased period (Fig. 4 *A*), as reported experimentally (3). In contrast, in the WT strain the glucose-dependent repression of *wc-1* transcription by CSP-1 counteracts increased expression of the *wc-1* gene at high glucose levels and the period remains constant (3).

2. SUPPORTING FIGURES

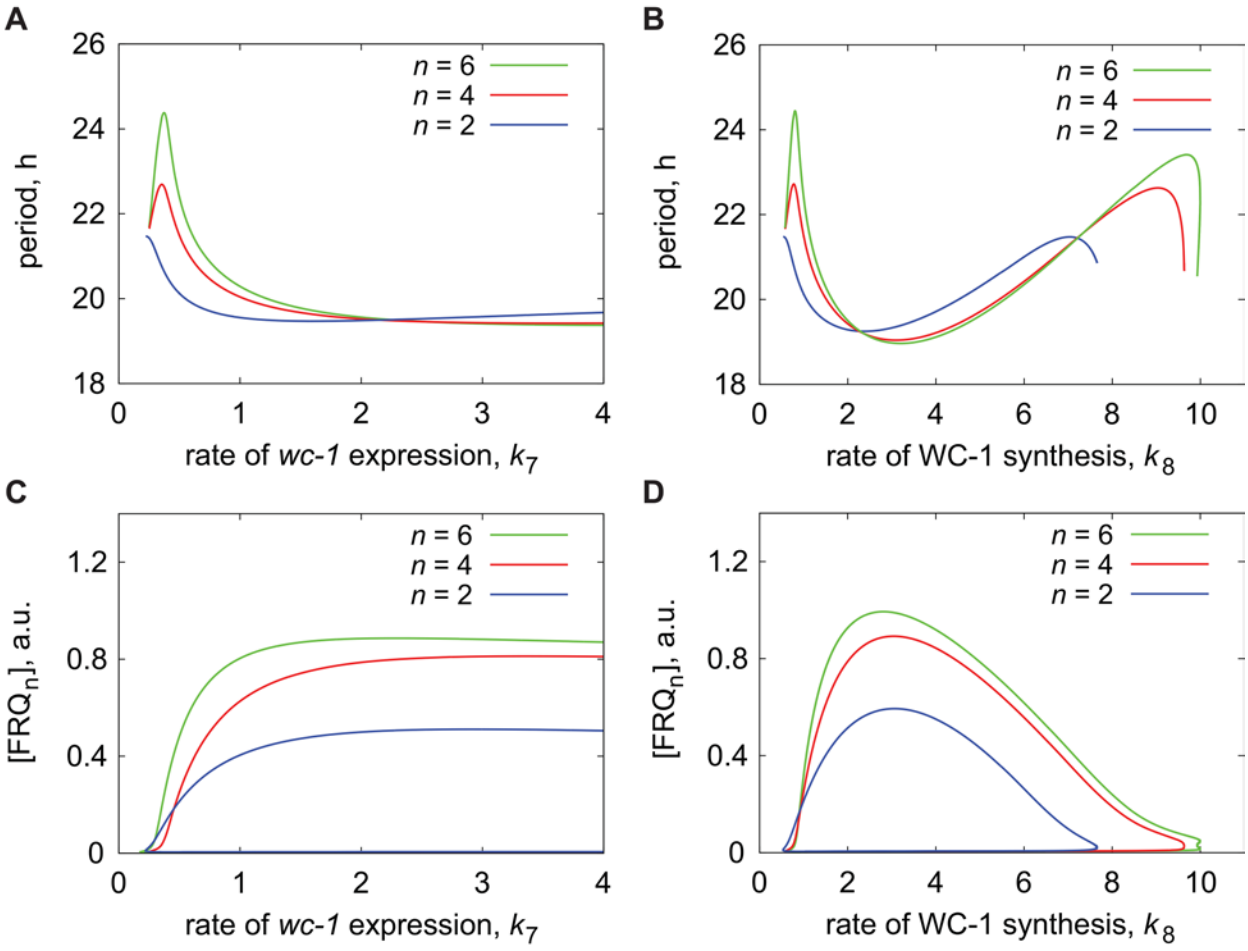

FIGURE S1 Period change and FRQ_n abundance with increasing Hill coefficient of WC-1 binding at the *frq* promoter. *(A)* Clock period and *(C)* envelope (max and min) of FRQ_n oscillations in the model with the increase of the *wc-1* expression rate constant k_7. *(B)* Clock period and *(D)* FRQ_n envelope (max and min) in the model with the increase of the WC-1 synthesis rate constant k_8. The Hill coefficient of WC-1 binding at the *frq* promoter is color coded (n = 2, 4 and 6).

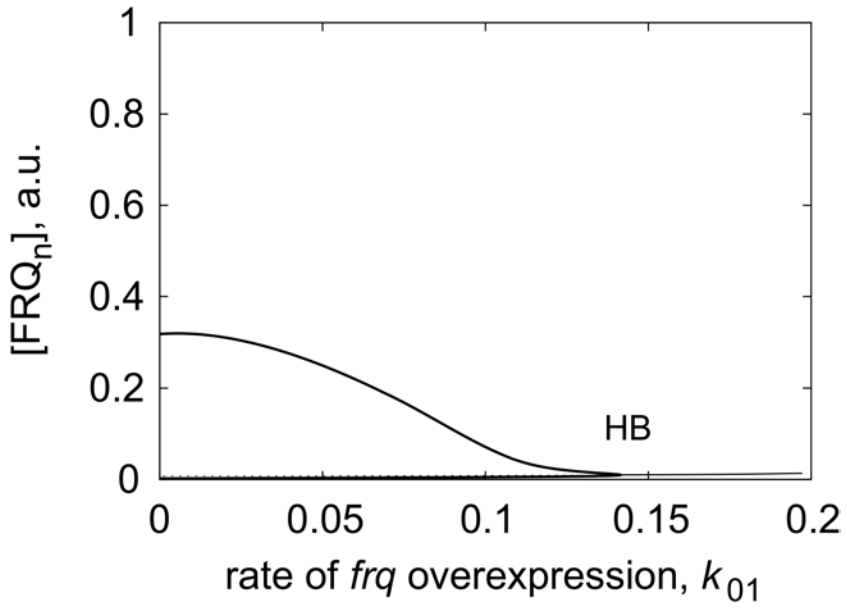

FIGURE S2 FRQ_n abundance in a simulated *frq* overexpression experiment in wild type genetic background. A bifurcation diagram showing the envelope (max and min) of FRQ_n oscillations (*thick solid curve*) as a function of the rate of *frq* overexpression, k_{01}. Oscillations disappear via a supercritical Hopf bifurcation (HB). The thin curve represents an unstable steady state. Parameter values are as described in Material and Methods.

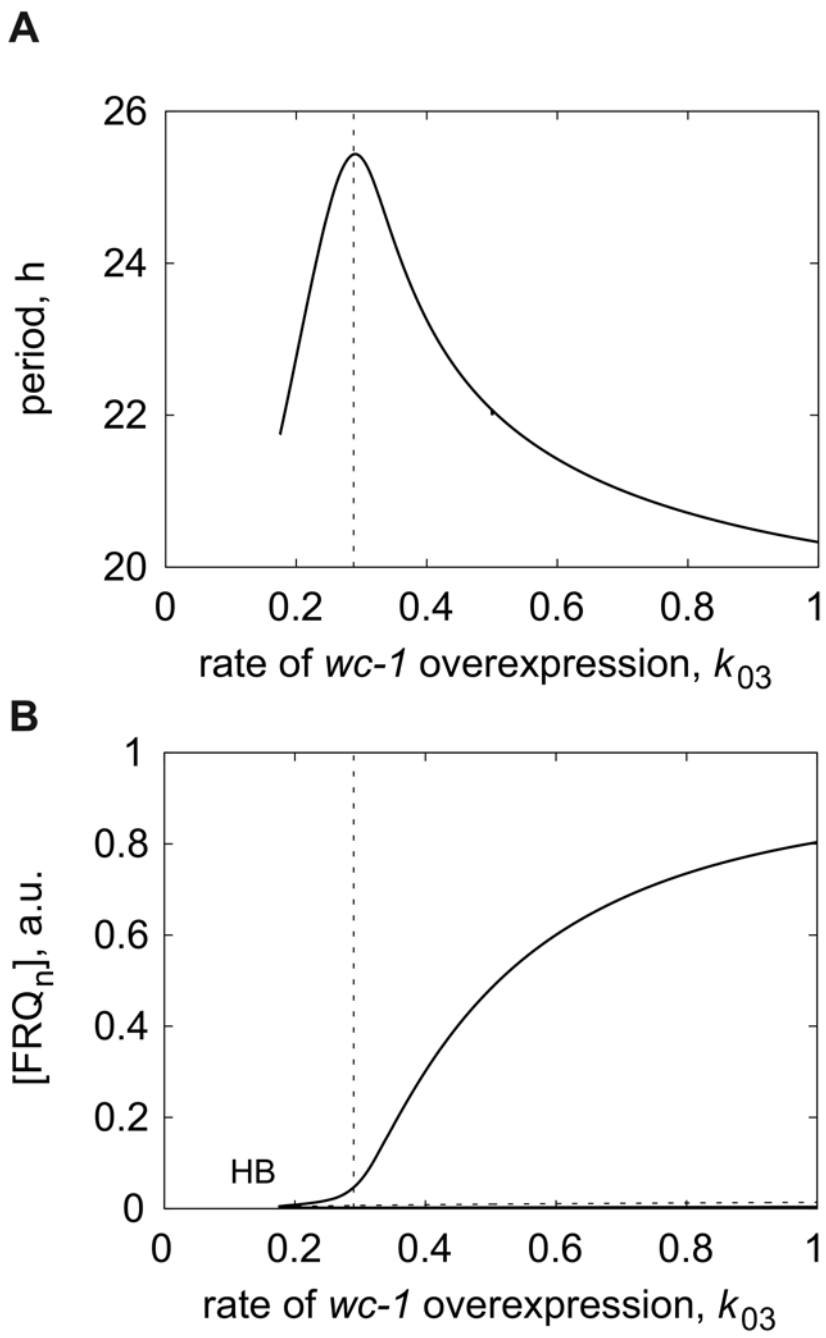

FIGURE S3 Clock period and FRQ_n abundance in a simulated *wc-1* overexpression experiment in *wc-1*^{ko} genetic background. *(A)* Period as a function of *wc-1* overexpression rate k_{03}. *(B)* A bifurcation diagram showing the envelope (max and min) of FRQ_n oscillations (*thick solid curve*) as a function of k_{03}. Oscillations appear via a supercritical Hopf bifurcation (HB). Dashed vertical lines mark the parameter value corresponding to the peak in the period curve in *(A)*. The thin dotted curve in *(B)* represents an unstable steady state. The *wc-1* expression rate constant $k_7 = 0$.

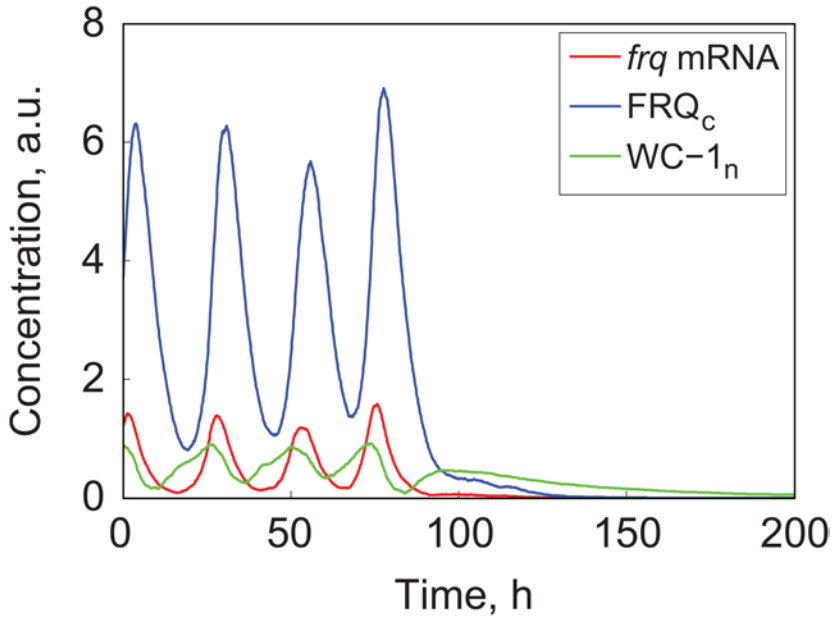

FIGURE S4 Die-out of oscillations in the stochastic version of the model in the presence of weak noise. When the circadian system is close to a Hopf bifurcation (Fig. S1), even a very weak noise may push the system into the basin of attraction of its co-existing steady state and oscillations would be lost. Time traces of *frq* mRNA, FRQ_c and $WC\text{-}1_n$ are shown. Parameter values are as described, except the *wc-1* expression rate constant $k_7 = 0$ and the *wc-1* overexpression rate $k_{03} = 0.26$. The volume factor of the stochastic simulations is $\Omega = 1000$.

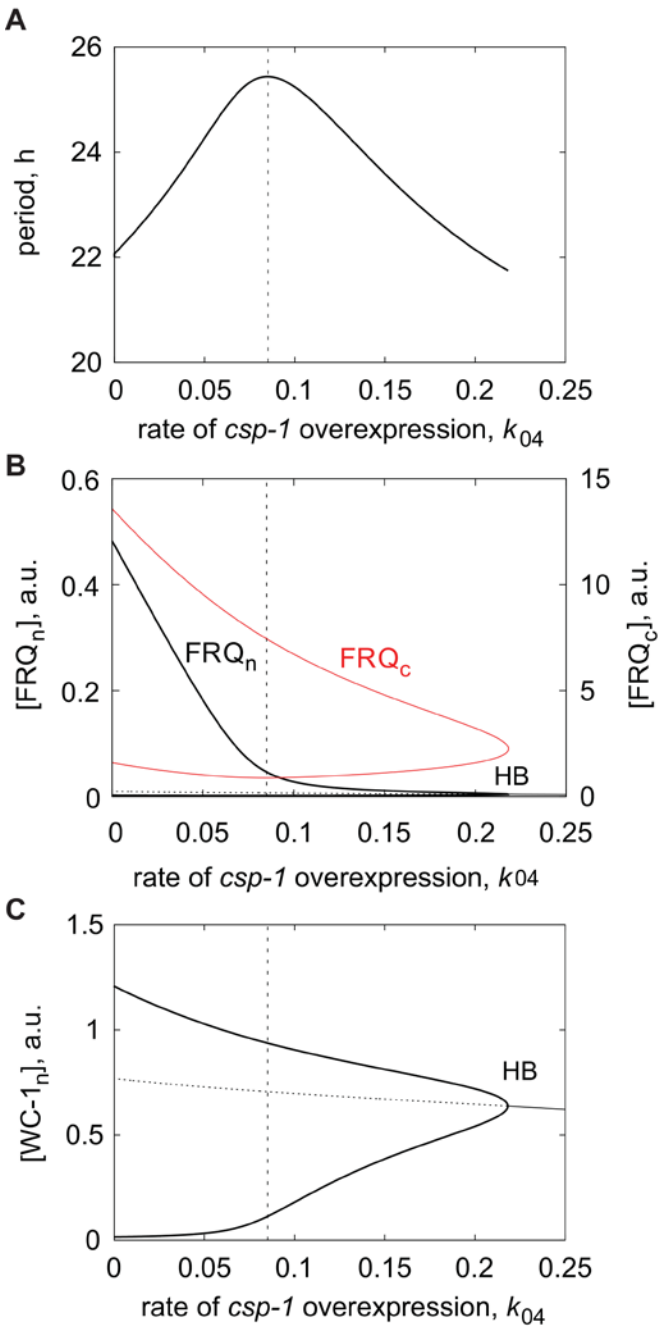

FIGURE S5 Period, FRQ_n and $WC\text{-}1_n$ levels in a simulated *csp-1* overexpression experiment. *(A)* Period as a function of the *csp-1* overexpression rate k_{04}. Bifurcation diagrams showing envelopes (max and min) of *(B)* FRQ_n (*black curve*) and FRQ_c (*red curve*) and *(C)* $WC\text{-}1_n$ oscillations (*thick solid curve*) as a function of k_{04}. Oscillations are lost via a supercritical Hopf bifurcation (HB). Thin solid (dotted) curves represent stable (unstable) steady states. Dashed vertical lines mark the parameter value corresponding to the peak in the period curve in *(A)*. Parameter values are as described in Materials and Methods, except the *csp-1* expression rate constant $k_{16} = 0$.

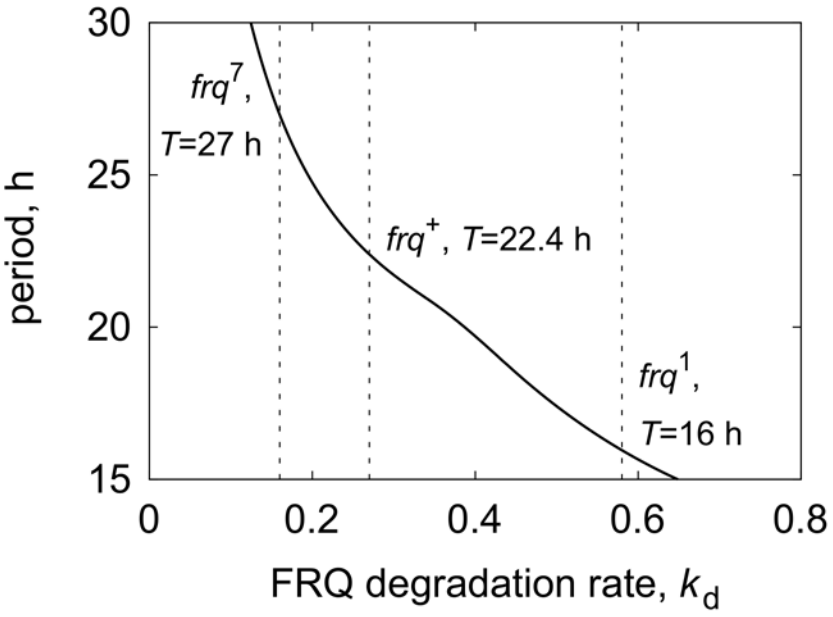

FIGURE S6 FRQ mutant alleles as simulated with varying the FRQ degradation rate. Vertical dashed lines mark FRQ degradation rate values corresponding to frq^7, frq^+ and frq^1 alleles as shown. The FRQ degradation rate k_d is defined as the rate of degradation of cytosolic and nuclear FRQ.

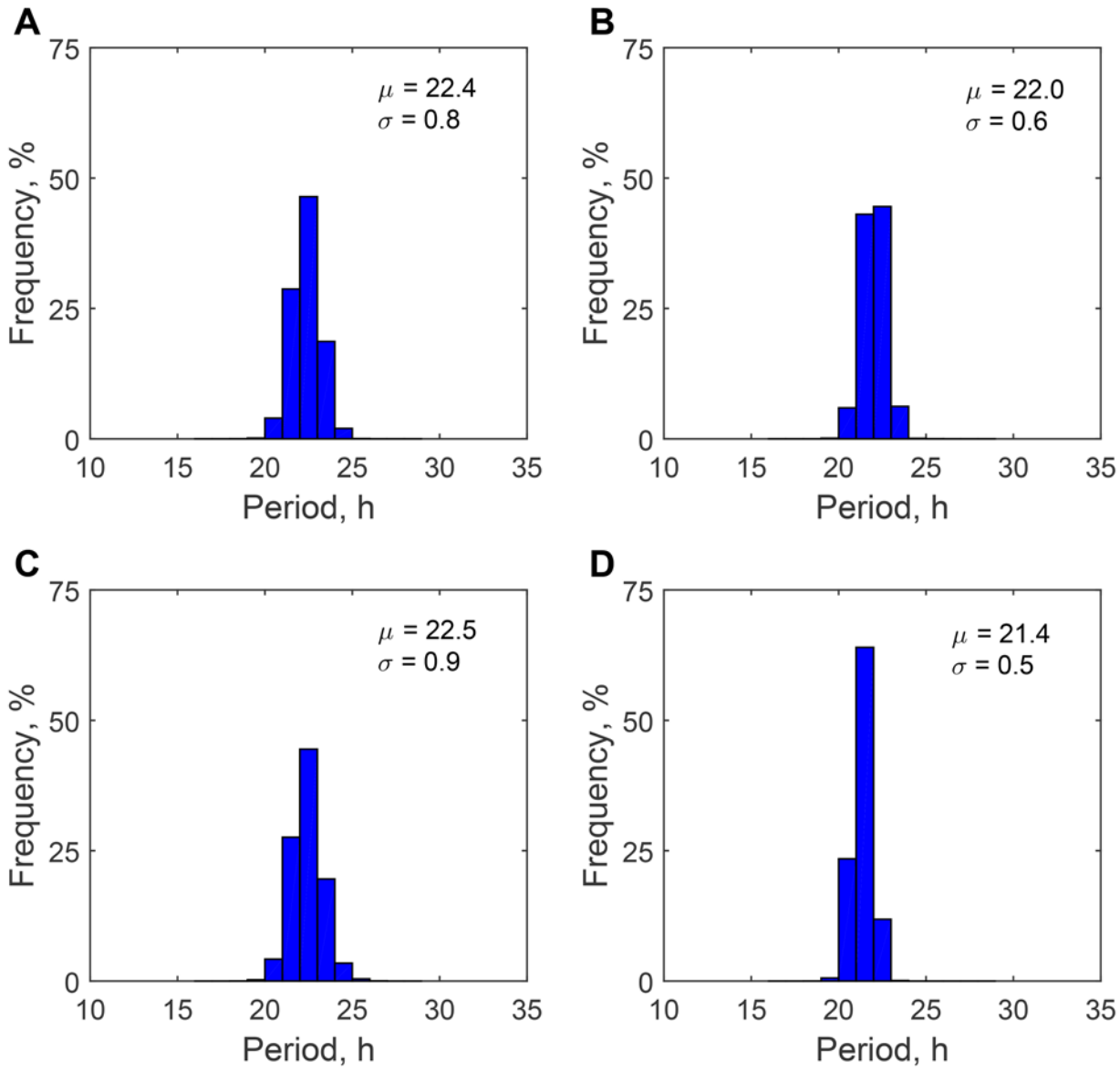

FIGURE S7 Histograms of period distributions obtained by stochastic simulations with weak noise. Period distributions in the presence of weak noise for the WT *(A, C)* and the *csp-1*^{ko} *(B, D)* in low and high glucose conditions, correspondingly. The histograms of periods of 10,000 cycles are computed from 100 simulation runs with 100 successive cycles with the volume factor Ω = 1000. The period was determined as the time interval separating two successive peaks of FRQ_c. The mean value (μ) and standard deviation (σ) of the period (in hours) is shown in each histogram. Parameter values are as described, except *(B)* $k_{16} = 0$, *(C)* $k_7 = 0.6$, $k_{16} = 0.57$ and *(D)* $k_7 = 0.6$, $k_{16} = 0$.

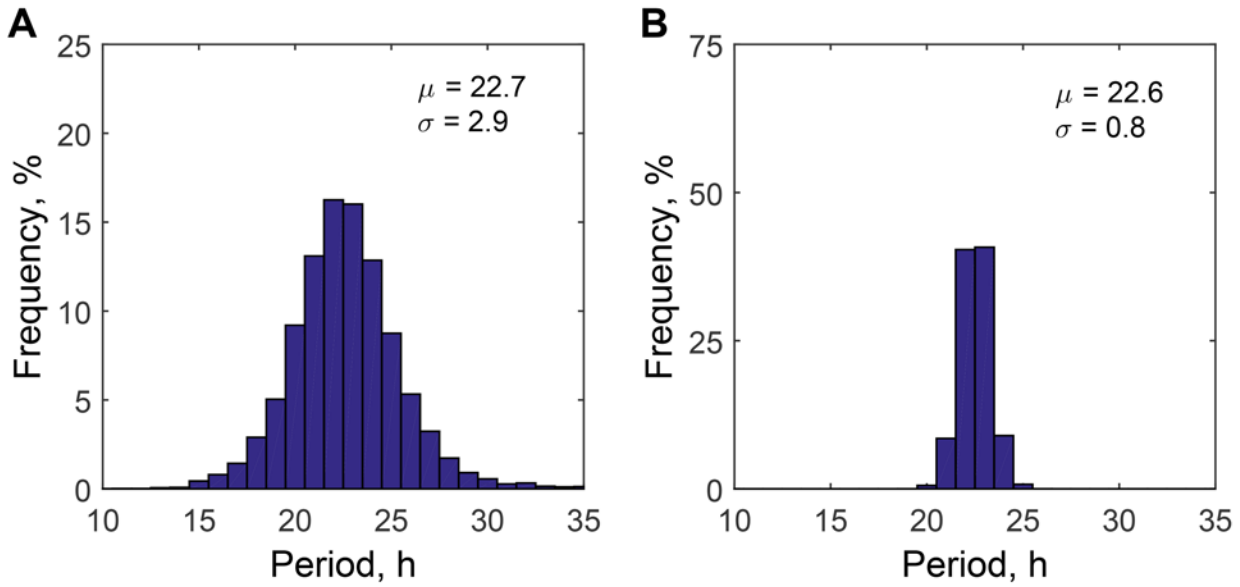

FIGURE S8 Histograms of period distributions obtained by stochastic simulations in a *csp-1*^{ko} parameter set in very low glucose. Period distributions in a *csp-1*^{ko} parameter set in very low glucose conditions in the presence of strong *(A)* or weak *(B)* noise. The histograms of periods of 10,000 cycles are computed from 100 simulation runs with 100 successive cycles with volume factors Ω = 100 *(A)* and Ω = 1000 *(B)*. The period was determined as the time interval separating two successive peaks of FRQ_c. The mean value (μ) and standard deviation (σ) of the period (in hours) is shown in each histogram. Parameter values are as described, except k_7 = 0.45, k_{16} = 0.

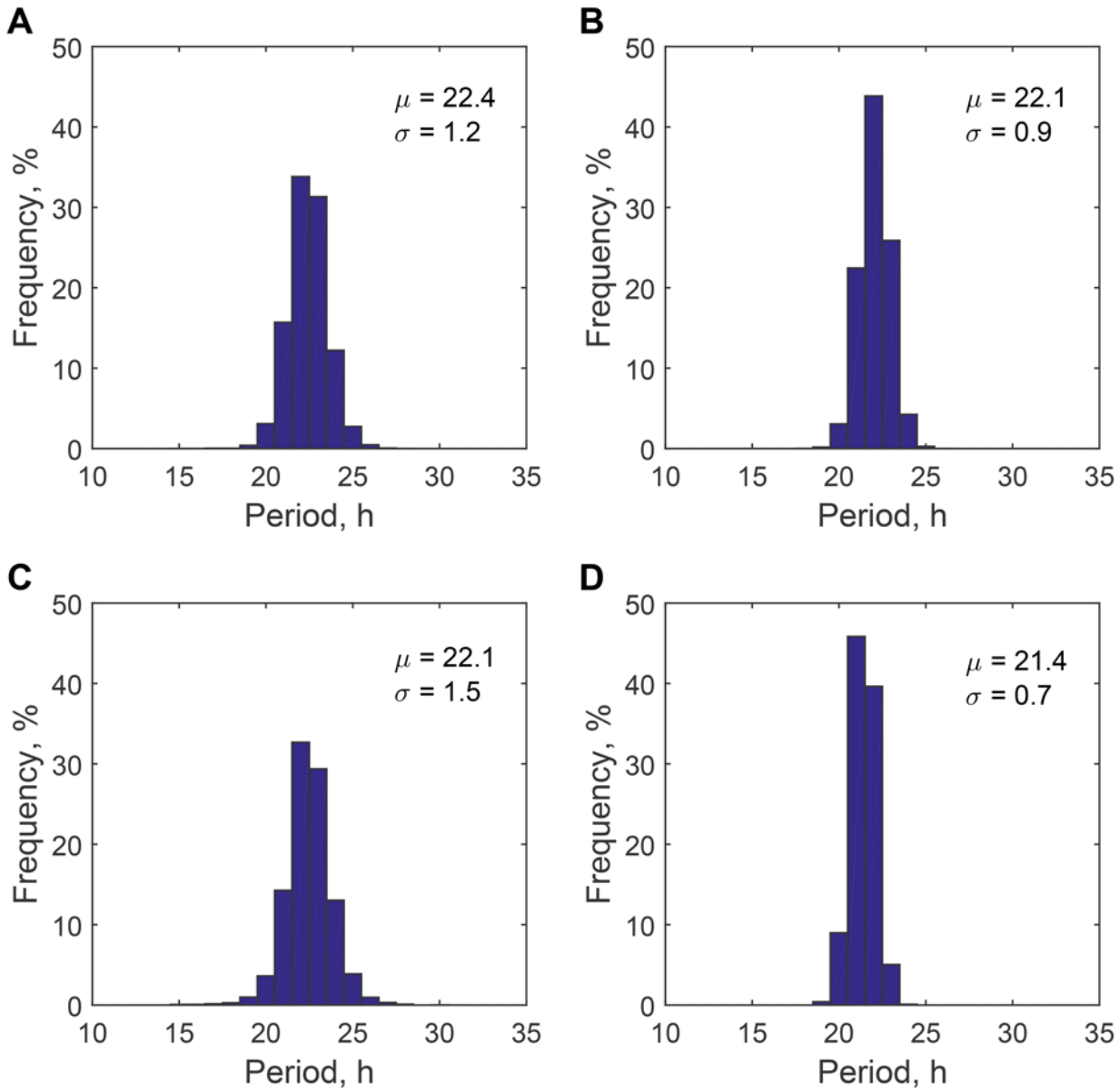

FIGURE S9 Histograms of period distributions obtained by rewriting the model equations as Langevin-type equations with multiplicative noise. Period distributions for the WT *(A, C)* and *csp-1*^{ko} *(B, D)* in low and high glucose conditions, correspondingly. Langevin-type equations have the form $dx_i/dt = f_i(...) + w_i(t)\sqrt{2D_i x_i}$, where $dx_i/dt = f_i(...)$ is the original deterministic equation, $w_i(t)$ is Gaussian white noise with zero mean and unit variance and $D_i = 0.0005$ is the noise amplitude that we kept the same for all variables. The histograms of periods of 10,000 cycles computed from 10 simulation runs with 1,000 successive cycles. The period was determined as the time interval separating two successive peaks of FRQ_c. The mean value (μ) and standard deviation (σ) of the period (in hours) is shown in each histogram. We obtain qualitatively similar results with the additive noise (not shown). Parameter values are as described, except *(B)* $k_{16} = 0$, *(C)* $k_7 = 0.6$, $k_{16} = 0.57$ and *(D)* $k_7 = 0.6$, $k_{16} = 0$.

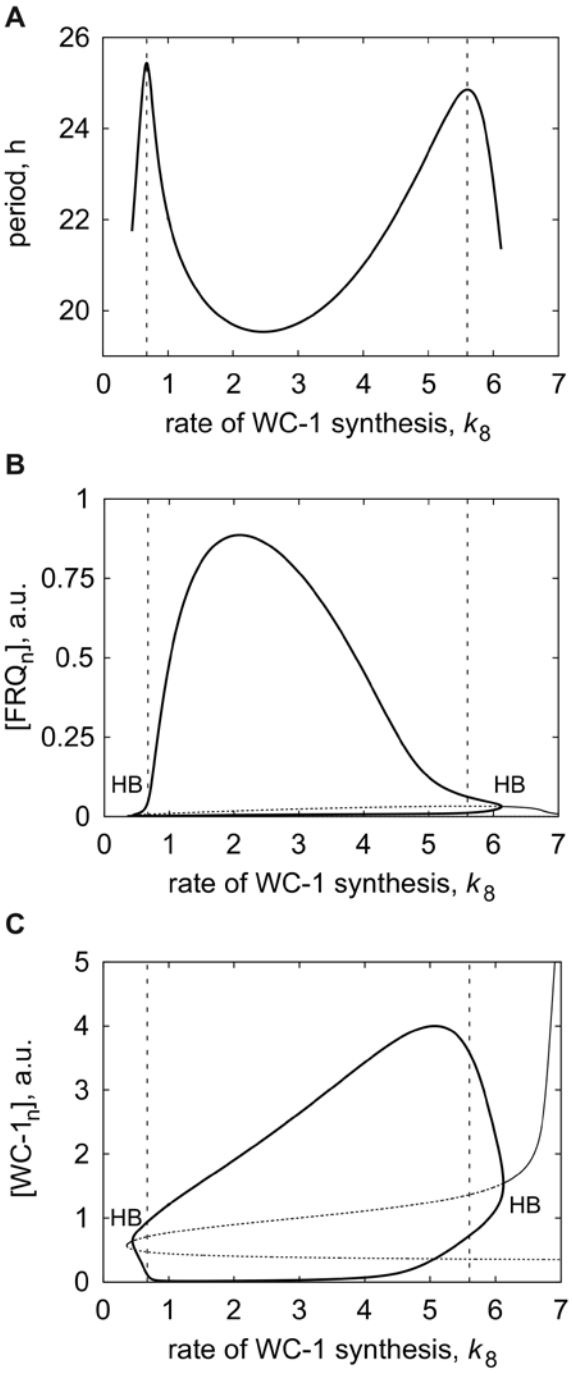

FIGURE S10 Clock period, FRQ_n and $WC\text{-}1_n$ levels in the *csp-1*^{ko} strain as a function of the WC-1 synthesis rate k_8. *(A)* The period as a function of k_8, simulating the increase in glucose concentration. One-parameter bifurcation diagrams show the envelopes (max and min) of *(B)* FRQ_n and *(C)* $WC\text{-}1_n$ oscillations (*thick solid curve*) as a function of k_8. Oscillatory regions are bounded by supercritical Hopf bifurcations (HB). Thin solid (dotted) curves represent stable (unstable) steady states. Dashed vertical lines mark the parameter values corresponding to the peaks in the period curve in *(A)*. Parameter values are as described, except $k_{16} = 0$.

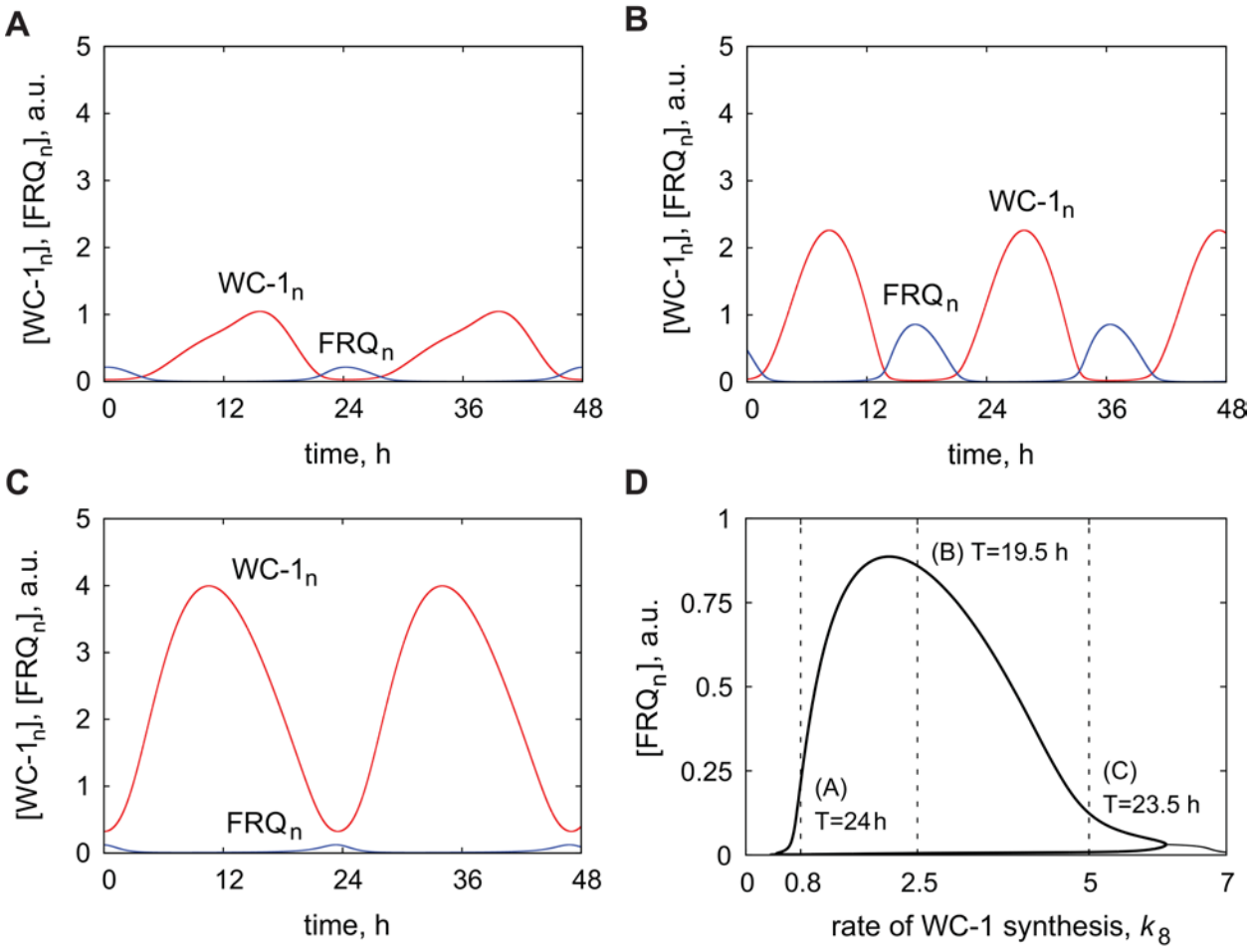

FIGURE S11 Oscillatory profiles of FRQ_n and $WC\text{-}1_n$ levels in the *csp-1*^{ko} strain with the increase in the WC-1 translation rate, k_8. *(A-C)* Oscillatory profiles of FRQ_n and $WC\text{-}1_n$ at different values of the WC-1 translation rate, k_8. *(D)* A one-parameter bifurcation diagram showing a steady state level of FRQ_n (*thin solid curve*) and the envelope (max and min concentrations) of FRQ_n oscillations (*thick solid curve*) as a function of k_8. Dashed vertical lines mark the parameter values corresponding to oscillatory profiles in *(A-C)*. Circadian periods for oscillatory profiles in *(A-C)* are also given. Parameter values are as described, except the rate of *csp-1* expression, $k_{16} = 0$ and *(A)* $k_8 = 0.8$, *(B)* $k_8 = 2.5$, *(C)* $k_8 = 5$.

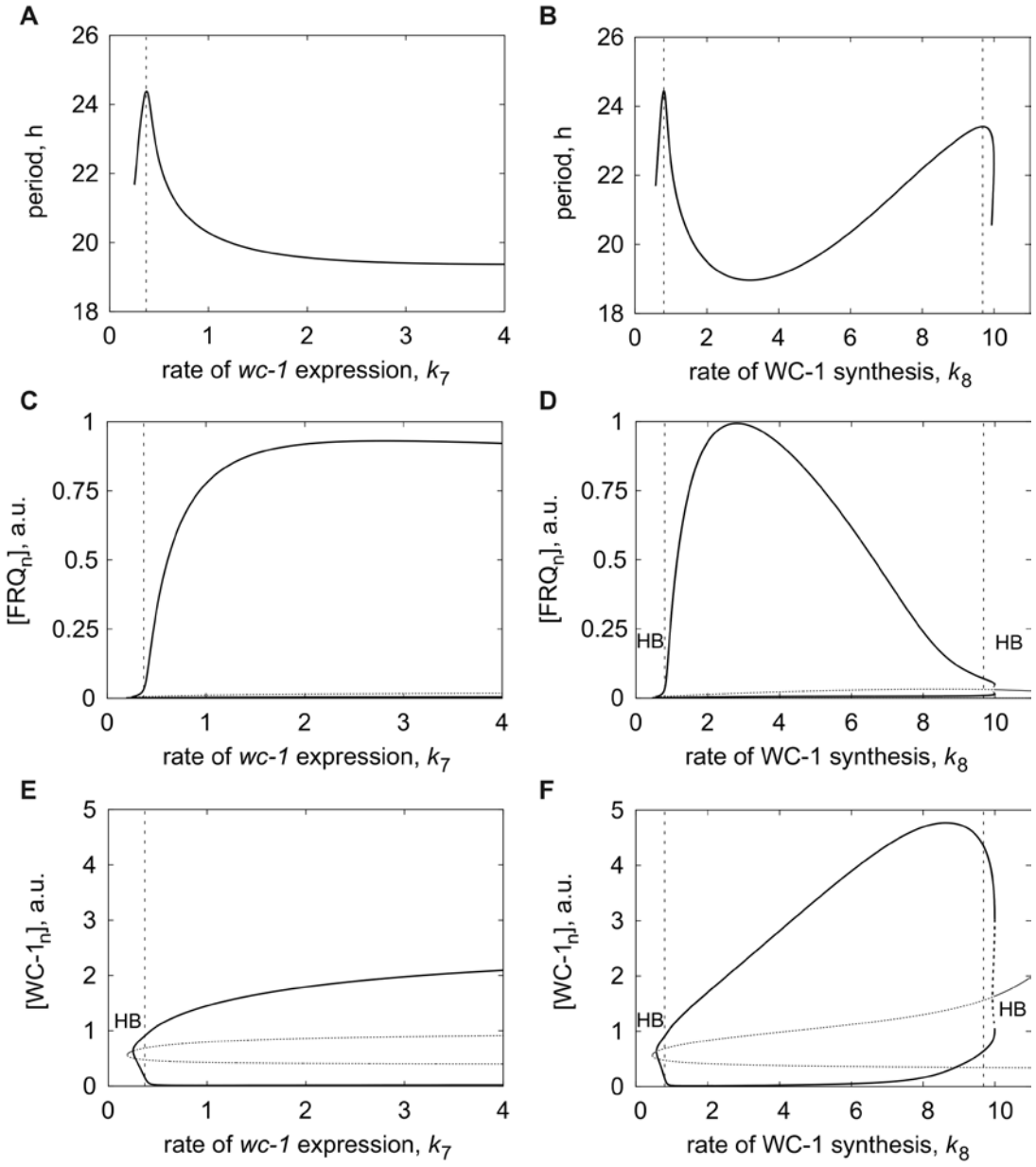

FIGURE S12 Simulated clock period, FRQ_n and $WC\text{-}1_n$ levels in the WT strain. *(A)* Clock period as a function of the *wc-1* expression rate constant k_7. *(B)* Clock period as a function of the WC-1 protein translation rate constant k_8. One-parameter bifurcation diagrams show the envelopes (max and min) of *(C)* FRQ_n and *(E)* $WC\text{-}1_n$ as a function of k_7. Oscillatory region in parameter k_7 is bounded by a supercritical Hopf bifurcation (HB) at the lower boundary. One-parameter bifurcation diagrams show the envelopes (max and min) of *(D)* FRQ_n and *(E)* $WC\text{-}1_n$ (*thick solid curve*) as a function of k_8. An oscillatory region in parameter k_8 is bounded by two supercritical Hopf bifurcations (HB). Dashed thick curves represent unstable oscillatory solutions, and thin solid (dotted) curves represent stable (unstable) steady states. Dashed vertical lines mark the parameter values corresponding to the peaks in the period curves in *(A)* and *(B)*.

3. SUPPORTING TABLES

TABLE S1 Reactions and probabilities for the stochastic formulation of the model. The second column provides the list of all reactions that occur in the model. The third column gives the probability of each reaction to occur. The change in the number of molecules as a result of a particular reaction is shown in the last column. G, H and I represent *frq*, *wc-1* and *csp-1* genes, correspondingly. Note that we do not decompose the terms of the deterministic model into detailed reaction steps.

Reaction number	Reaction	Probability of reaction	Transition
1	G $\rightarrow$ *frq* mRNA + G	$w_1 = (k_1\Omega)\dfrac{\text{WC-1}_\text{n}^{\,6}}{K\Omega^6 + \text{WC-1}_\text{n}^{\,6}}$	*frq* mRNA $\rightarrow$ *frq* mRNA + 1
2	*frq* mRNA $\rightarrow$	$w_2 = k_4 frq$ mRNA	*frq* mRNA $\rightarrow$ *frq* mRNA – 1
3	*frq* mRNA $\rightarrow$ FRQ_c + *frq* mRNA	$w_3 = k_2 frq$ mRNA	$\text{FRQ}_\text{c} \rightarrow \text{FRQ}_\text{c} + 1$
4	$\text{FRQ}_\text{c} \rightarrow \text{FRQ}_\text{n}$	$w_4 = k_3\text{FRQ}_\text{c}$	$\text{FRQ}_\text{c} \rightarrow \text{FRQ}_\text{c} - 1$ $\text{FRQ}_\text{n} \rightarrow \text{FRQ}_\text{n} + 1$
5	$\text{FRQ}_\text{c} \rightarrow$	$w_5 = k_5\text{FRQ}_\text{c}$	$\text{FRQ}_\text{c} \rightarrow \text{FRQ}_\text{c} - 1$
6	FRQ_n:$\text{WC-1}_\text{n} \rightarrow$ FRQ_n + WC-1_n	$w_6 = k_{14}\text{FRQ}_\text{n}$:$\text{WC-1}_\text{n}$	$\text{FRQ}_\text{n} \rightarrow \text{FRQ}_\text{n} + 1$ $\text{WC-1}_\text{n} \rightarrow \text{WC-1}_\text{n} + 1$ FRQ_n:$\text{WC-1}_\text{n} \rightarrow$ FRQ_n:$\text{WC-1}_\text{n} - 1$
7	$\text{FRQ}_\text{n} \rightarrow$	$w_7 = k_6\text{FRQ}_\text{n}$	$\text{FRQ}_\text{n} \rightarrow \text{FRQ}_\text{n} - 1$
8	FRQ_n + $\text{WC-1}_\text{n} \rightarrow$ FRQ_n:WC-1_n	$w_8 = (k_{13}/\Omega)\text{FRQ}_\text{n}\text{WC-1}_\text{n}$	$\text{FRQ}_\text{n} \rightarrow \text{FRQ}_\text{n} - 1$ $\text{WC-1}_\text{n} \rightarrow \text{WC-1}_\text{n} - 1$ FRQ_n:$\text{WC-1}_\text{n} \rightarrow$ FRQ_n:$\text{WC-1}_\text{n} + 1$
9	H $\rightarrow$ *wc-1* mRNA + H	$w_9 = (k_7\Omega)\dfrac{K_1\Omega}{K_1\Omega + \text{CSP-1}}$	*wc-1* mRNA $\rightarrow$ *wc-1* mRNA + 1
10	*wc-1* mRNA $\rightarrow$	$w_{10} = k_{10} wc\text{-}1$ mRNA	*wc-1* mRNA $\rightarrow$ *wc-1* mRNA – 1

11	*wc-1* mRNA → WC-1_c + *wc-1* mRNA	$w_{11} = (k_8\Omega)\frac{\text{FRQ}_\text{c}^{\,2}}{K_2\Omega^2 + \text{FRQ}_\text{c}^{\,2}} \cdot \frac{wc\text{-1 mRNA}}{K_3\Omega + wc\text{-1 mRNA}}$	WC-1_c → WC-1_c + 1
12	WC-1_c → WC-1_n	$w_{12} = k_9\text{WC-1}_\text{c}$	WC-1_c → WC-1_c – 1 WC-1_n → WC-1_n + 1
13	WC-1_c →	$w_{13} = k_{11}\text{WC-1}_\text{c}$	WC-1_c → WC-1_c – 1
14	WC-1_n →	$w_{14} = k_{12}\text{WC-1}_\text{n}$	WC-1_n → WC-1_n – 1
15	FRQ_n:WC-1_n →	$w_{15} = k_{15}\text{FRQ}_\text{n}$:$\text{WC-1}_\text{n}$	FRQ_n:WC-1_n → FRQ_n:WC-1_n – 1
16	I → *csp-1* mRNA + I	$w_{16} = k_{16}\text{WC-1}_\text{n}\frac{K_4\Omega}{K_4\Omega + \text{CSP-1}}$	*csp-1* mRNA → *csp-1* mRNA + 1
17	*csp-1* mRNA →	$w_{17} = k_{17}csp\text{-1 mRNA}$	*csp-1* mRNA → *csp-1* mRNA – 1
18	*csp-1* mRNA → CSP-1 + *csp-1* mRNA	$w_{18} = k_{18}csp\text{-1 mRNA}$	CSP-1 → CSP-1 + 1
19	CSP-1 →	$w_{19} = k_{19}\text{CSP-1}$	CSP-1 → CSP-1 – 1

SUPPORTING REFERENCES

1. Yu, Y., W. Dong, C. Altimus, X. Tang, J. Griffith, M. Morello, L. Dudek, J. Arnold, and H. B. Schuttler. 2007. A genetic network for the clock of Neurospora crassa. Proceedings of the National Academy of Sciences of the United States of America 104:2809-2814.
2. Cheng, P., Y. Yang, and Y. Liu. 2001. Interlocked feedback loops contribute to the robustness of the Neurospora circadian clock. Proceedings of the National Academy of Sciences of the United States of America 98:7408-7413.
3. Sancar, G., C. Sancar, and M. Brunner. 2012. Metabolic compensation of the Neurospora clock by a glucose-dependent feedback of the circadian repressor CSP1 on the core oscillator. Genes & development 26:2435-2442.
4. Cheng, P., Y. Yang, C. Heintzen, and Y. Liu. 2001. Coiled-coil domain-mediated FRQ-FRQ interaction is essential for its circadian clock function in Neurospora. The EMBO journal 20:101-108.
5. Garceau, N. Y., Y. Liu, J. J. Loros, and J. C. Dunlap. 1997. Alternative initiation of translation and time-specific phosphorylation yield multiple forms of the essential clock protein FREQUENCY. Cell 89:469-476.
6. Lee, K., J. J. Loros, and J. C. Dunlap. 2000. Interconnected feedback loops in the Neurospora circadian system. Science 289:107-110.
7. Hong, C. I., I. W. Jolma, J. J. Loros, J. C. Dunlap, and P. Ruoff. 2008. Simulating dark expressions and interactions of frq and wc-1 in the Neurospora circadian clock. Biophysical journal 94:1221-1232.